File Cy

BRL MR 2597

BRL

MEMORANDUM REPORT NO. 2597

(Partially supersedes IMR No. 190)

CONTAINMENT STRUCTURES VERSUS SUPPRESSIVE STRUCTURES

Norris J. Huffington, Jr.
Struan R. Robertson

February 1976

USA BALLISTIC RESEARCH LABORATORIES
ABERDEEN PROVING GROUND, MARYLAND

Destroy this report when it is no longer needed.
Do not return it to the originator.

Secondary distribution of this report by originating or sponsoring activity is prohibited.

Additional copies of this report may be obtained from the National Technical Information Service, U.S. Department of Commerce, Springfield, Virginia 22151.

The findings in this report are not to be construed as an official Department of the Army position, unless so designated by other authorized documents.

UNCLASSIFIED

SECURITY CLASSIFICATION OF THIS PAGE *(When Data Entered)*

REPORT DOCUMENTATION PAGE		READ INSTRUCTIONS BEFORE COMPLETING FORM
1. REPORT NUMBER BRL MEMORANDUM REPORT NO. 2597	2. GOVT ACCESSION NO.	3. RECIPIENT'S CATALOG NUMBER
4. TITLE *(and Subtitle)* CONTAINMENT STRUCTURES VERSUS SUPPRESSIVE STRUCTURES		5. TYPE OF REPORT & PERIOD COVERED Final 6. PERFORMING ORG. REPORT NUMBER
7. AUTHOR*(s)* Norris J. Huffington, Jr. Struan R. Robertson		8. CONTRACT OR GRANT NUMBER*(s)*
9. PERFORMING ORGANIZATION NAME AND ADDRESS USA Ballistic Research Laboratories Aberdeen Proving Ground, Maryland 21005		10. PROGRAM ELEMENT, PROJECT, TASK AREA & WORK UNIT NUMBERS RDT&E 1W161102AH43
11. CONTROLLING OFFICE NAME AND ADDRESS U.S. Army Materiel Development & Readiness Command 5001 Eisenhower Avenue Alexandria, Virginia 22333		12. REPORT DATE FEBRUARY 1976 13. NUMBER OF PAGES 39
14. MONITORING AGENCY NAME & ADDRESS*(if different from Controlling Office)*		15. SECURITY CLASS. *(of this report)* UNCLASSIFIED 15a. DECLASSIFICATION/DOWNGRADING SCHEDULE

16. DISTRIBUTION STATEMENT *(of this Report)*

Approved for public release; distribution unlimited.

17. DISTRIBUTION STATEMENT *(of the abstract entered in Block 20, if different from Report)*

18. SUPPLEMENTARY NOTES

Partially supersedes IMR No. 190.

19. KEY WORDS *(Continue on reverse side if necessary and identify by block number)*

Suppressive Structures
Containment Structures
Structural Shells
Elastoplastic Response
Internal Blast
Hemispherical Shell
Cylindrical Shell

20. ABSTRACT *(Continue on reverse side if necessary and identify by block number)* (mba)

As part of a study of the suppressive structure concept, analyses of the large deflection, elastoplastic response of two configurations (a hemispherical shell and a cylindrical shell with closed ends) subjected to internal blast were performed. These blast and fragment containment structures may be regarded as limiting cases of suppressive structures and the results obtained are believed to constitute useful baseline data for evaluating efficiency of suppressive structure designs. The results indicate that these simple structures can provide total containment of fragments and blast for significantly less weight

DD FORM 1 JAN 73 1473 EDITION OF 1 NOV 65 IS OBSOLETE

(Continued)

UNCLASSIFIED

SECURITY CLASSIFICATION OF THIS PAGE *(When Data Entered)*

(Item 20 Continued)

and cost than a corresponding vented suppressive structure. Suggestions regarding more practical containment/suppressive structural configurations are included.

FOREWORD

This report is intended to supersede both Chapter VI of BRL Interim Memorandum Report No. 190 and the portion of Chapter VII concerned with structural response.

TABLE OF CONTENTS

I. INTRODUCTION

The concept of a suppressive structure entails the use of multi-component panels which are supported by a relatively rigid bent-type framework. The complete structure, consisting of framework plus panels, is fabricated from commercial low carbon steel and forms an enclosure surrounding the region where an accidental explosion may occur. The panels consist of arrays of bar elements (angles, zees, etc.), perforated plates, and louvred plates at various spacings. These panels are intended to provide total containment of fragments and to permit a restricted venting of the contained blast, resulting in a significant decrease in external overpressures over what would be realized if no suppressive structure were present. For an optimum design the entire structure would experience limited elastoplastic deformation, thus providing a sink for the released explosive energy.

To formulate a rigorous mathematical model for the response of such a complex structure and to develop efficient methods for obtaining numerical solutions would be extremely tedious and costly. However, such structures have been produced through a combination of approximate analytical procedures plus proof testing. In response to a request for short-term assistance in assessing the cost effectiveness of the suppressive structure concept it was decided to eschew any detailed modeling of such complex structures and to treat an idealized configuration whose response could be readily analyzed by an existing large deflection elastoplastic structural shell response computer program, PETROS 3.5.[1] This analytical tool would be employed to design an efficient closed (total containment) shell structure which would have the same protective capacity as an existing suppressive structure which was developed for application to an 81 mm mortar round automated assembly facility.[2] This suppressive structure is a welded steel framework 20 feet (6.10m) long by 15 feet (4.57m) wide by 13 feet (3.96m) high having 4 feet (1.22m) by 12 feet (3.66m) wall panels and 4 feet (1.22m) square ceiling panels, the total weight being 51000 pounds (226859N). The comparison between the total containment and suppressive structural designs should be meaningful because the suppressive structure, while not necessarily optimized, was certainly not grossly overdesigned (a fragment nearly perforated an outer louvred panel and the whole structure experienced appreciable permanent deformation).

---

[1] *S.D. Pirotin, B.A. Berg, and E.A. Witner, "PETROS 3.5: New Developments and Program Manual for the Finite-Difference Calculation of Large Elastic-Plastic Transient Deformations of Multilayer Variable-Thickness Shells," U.S. Army Ballistic Research Laboratories Contract Report No. 211, February 1975. AD# A007215.*

[2] *"Design, Fabrication and Test of a Suppressive Structure for Application to an 81 mm Mortar Round Automated Assembly Facility," Draft Report, Edgewood Arsenal Resident Office, National Aeronautics and Space Administration, Bay St. Louis, MS, 9 January 1974.*

II. ANALYSIS OF TOTAL CONTAINMENT STRUCTURE

A. Hemispherical Configuration

To achieve nearly homogeneous elastoplastic straining a hemispherical configuration was selected, this to be bolted down to a horizontal rigid foundation as shown in Figure 1. In the analysis this edge condition was treated as a clamped boundary. As was the case for the suppressive structure of Reference 2, this configuration must survive the simultaneous detonation of two 81 mm mortar rounds. For simplicity in the analysis, these rounds were located at a central point on the foundation so that the blast loading is spherically symmetric. The mathematical problem may now be posed as follows: For a shell thickness h determined by the requirement for fragment containment,* how small can the midsurface radius R of the hemisphere be made without causing structural failure due to blast loading?

In order to solve this problem it was necessary to formulate the pressure pulse as a function of the radius R. Data for this formulation are presented in Reference 3. For a selected value of R the pressure experienced by the target is represented in the following manner. At the arrival of the blast wave there is a jump to the peak reflected pressure, followed by an exponential decay which is terminated when the thermodynamic equilibrium pressure corresponding to the release of detonation energy and explosion products in a constant volume process is reached. Subsequent to this the pressure is taken to remain essentially constant at the equilibrium pressure. The actual loading pulse employed is illustrated in Figure 2 for the case R = 5 feet (1.52 m).

The material was taken to be 1020 steel, which was represented in the analysis as a strain hardening material with stress-strain properties modeled by the succession of linear segments shown in Figure 3. Strain-rate effects were neglected, which is conservative since these effects increase the structural resistance and thus reduce the total deformation.

The foregoing numerical quantities which have been discussed are the only physical data input required for the PETROS 3.5 code (Reference 1), which treats the transient response of shells by obtaining a finite difference solution of the nonlinear partial differential equations of motion. Since the loading and response are axisymmetric it is only necessary to use three meridional rows of mesh points. Owing to the highly nonlinear character of this transient response problem it is

---

For this case, h = 1 inch (25.4mm) of steel is sufficient, as discussed in Reference 3.

[3]*B. Bertrand, C. Brown, D. Dunn, N. Huffington, J. Kineke, C. Kingery, R. Meissner, A. Ricchiazzi, S. Robertson, and R. Vitali, "Suppressive Structures - A Quick Look," BRL Interim Memorandum Report No. 190, February 1974.*

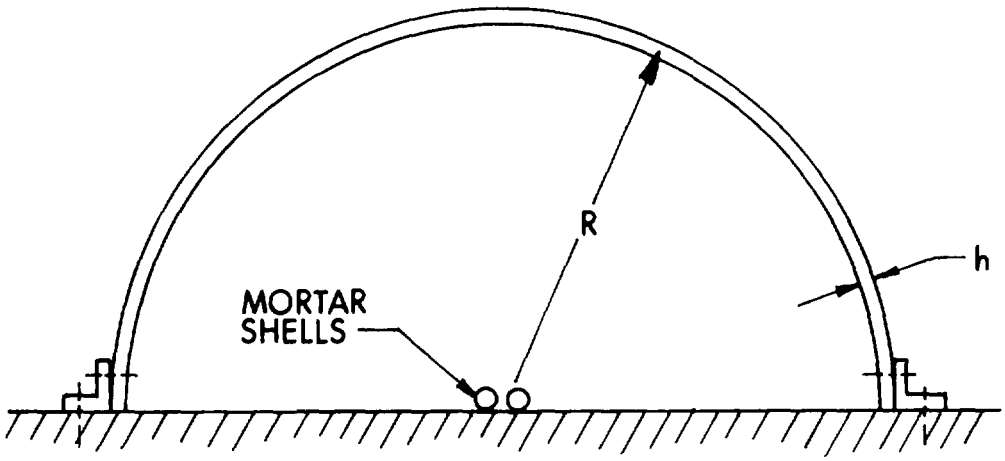

Figure 1. Section Through Hemispherical Containment Structure

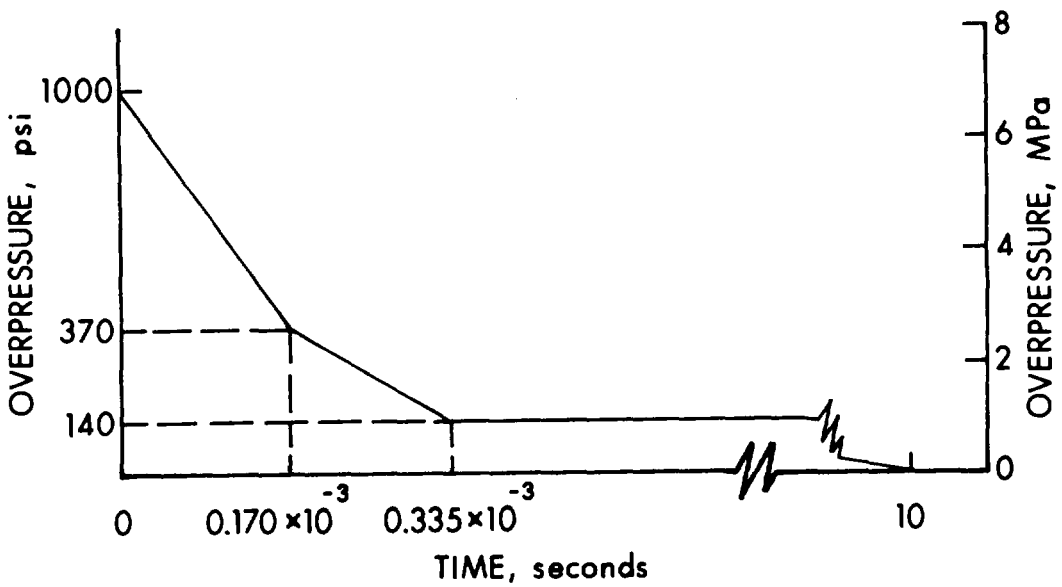

Figure 2. Blast Loading for R=5 Feet

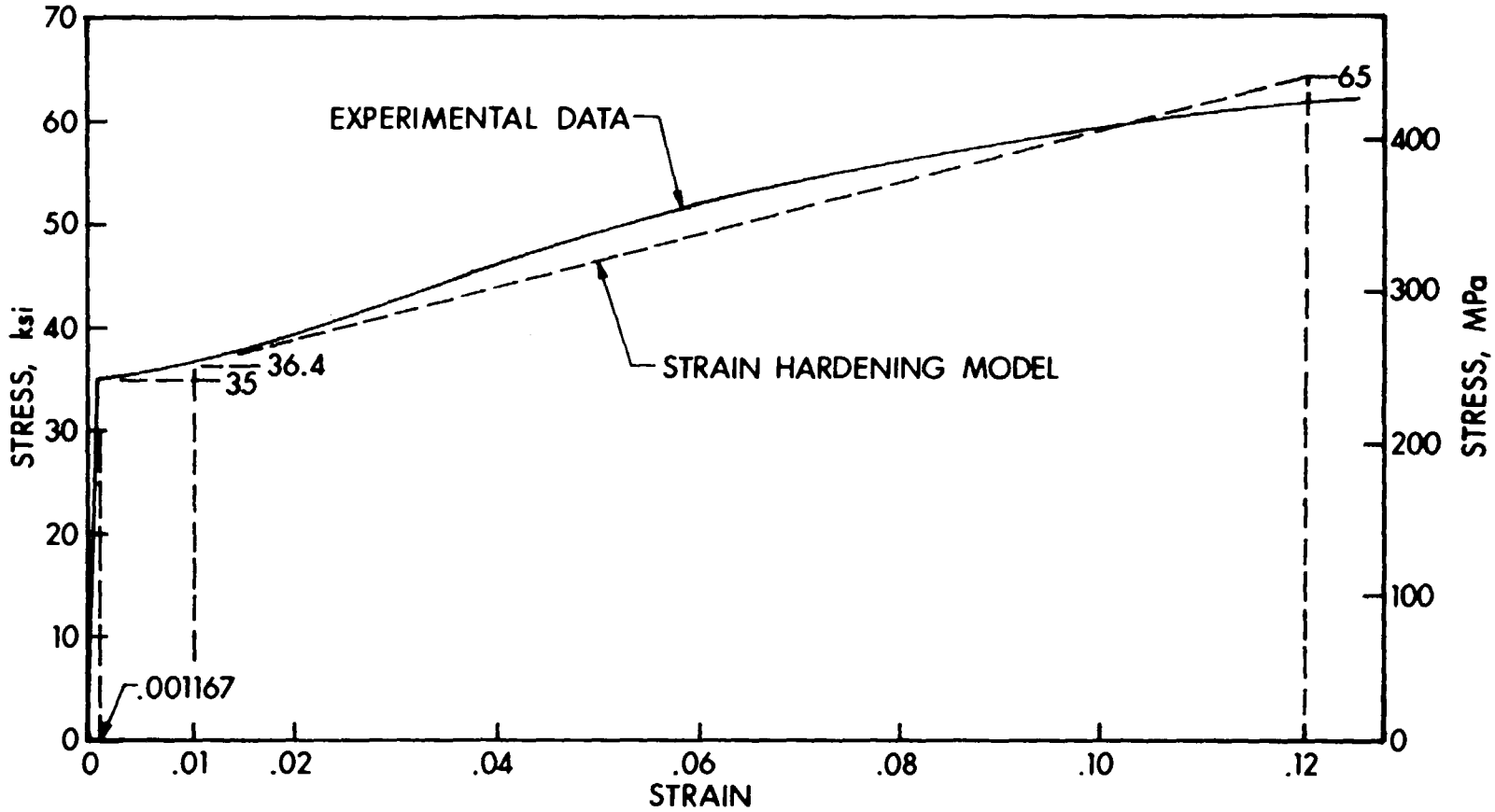

Figure 3. Stress-Strain Property Modeling

necessary to determine the minimum value for R by trial. When calculations were performed for R = 10 feet (3.05 m) the response was found to be entirely negligible. Results for R = 5 feet (1.52 m) are shown in the figures which follow. Figure 4 shows the transient rectangular components of displacement in a meridional plane at point A which is at 45° from the vertical axis of the hemisphere. From this it may be determined that the maximum displacement at this point is only 0.036 inches (0.914 mm), essentially radially outward. Displacements at other locations are correspondingly small except in the neighborhood of the pole of the hemisphere, where a significantly larger deflection develops after 4000 microseconds (as illustrated in Figure 5). This rather exceptional behavior in the vicinity of the pole led to a more extensive study of the solution of this problem which is reported in the Appendix. In this study it was determined that the deflections and strains in this structure remain everywhere small, which is consistent with the results shown in the energy balance diagram of Figure 6. This diagram, part of the graphrical output provided by the BRL version of the PETROS 3.5 code, shows the temporal variation of total energy and work quantities for the hemispherical shell. There is a gradual increase in the amount of (irreversible) plastic work but this will be bounded as the shell "shakes down" to purely elastic oscillations.

It has been noticed that the fluctuations of kinetic energy in this analysis have twice the frequency of the work performed by loads external to the structural shell (which are provided in this instance by the internal blast pressure). The explanation is relatively simple. Initially the hemisphere moves outward (except at the fixed boundary) in a "breathing" mode, the kinetic energy reaching a maximum value and then decreasing as the structural resistance becomes increasingly effective. At the maximum outward excursion the elastic strain energy is a maximum and the kinetic energy is a minimum (not zero because there is some kinetic energy of flexural vibration by this time). Up to this point the shell moved in the direction of the applied pressure loading so the external work was positive. The shell then moves inward, picking up speed until the kinetic energy reaches its second maximum and then slowing down as the internal stresses and the applied pressure become dominant. The second minimum of the kinetic energy occurs at approximately 1000 microseconds, corresponding to a relative maximum of the strain energy. During the inward motion of the shell work was performed by the shell against the internal pressure (negative work) which accounts for the decrease of the external work to a minimum at the same time as the second minimum of the kinetic energy. The shell then moves outwards and the preceding energy fluctuations are repeated cyclically. Although more energy is converted to flexural motions and plastic work as the solution proceeds, the frequencies associated with the breathing oscillations continue to be observable in the kinetic energy and external work plots.

From the above it may be inferred that the radius R of the hemisphere could be made considerably less than 5 feet (1.52 m) before danger of rupture would arise. However, to be conservative and because the size

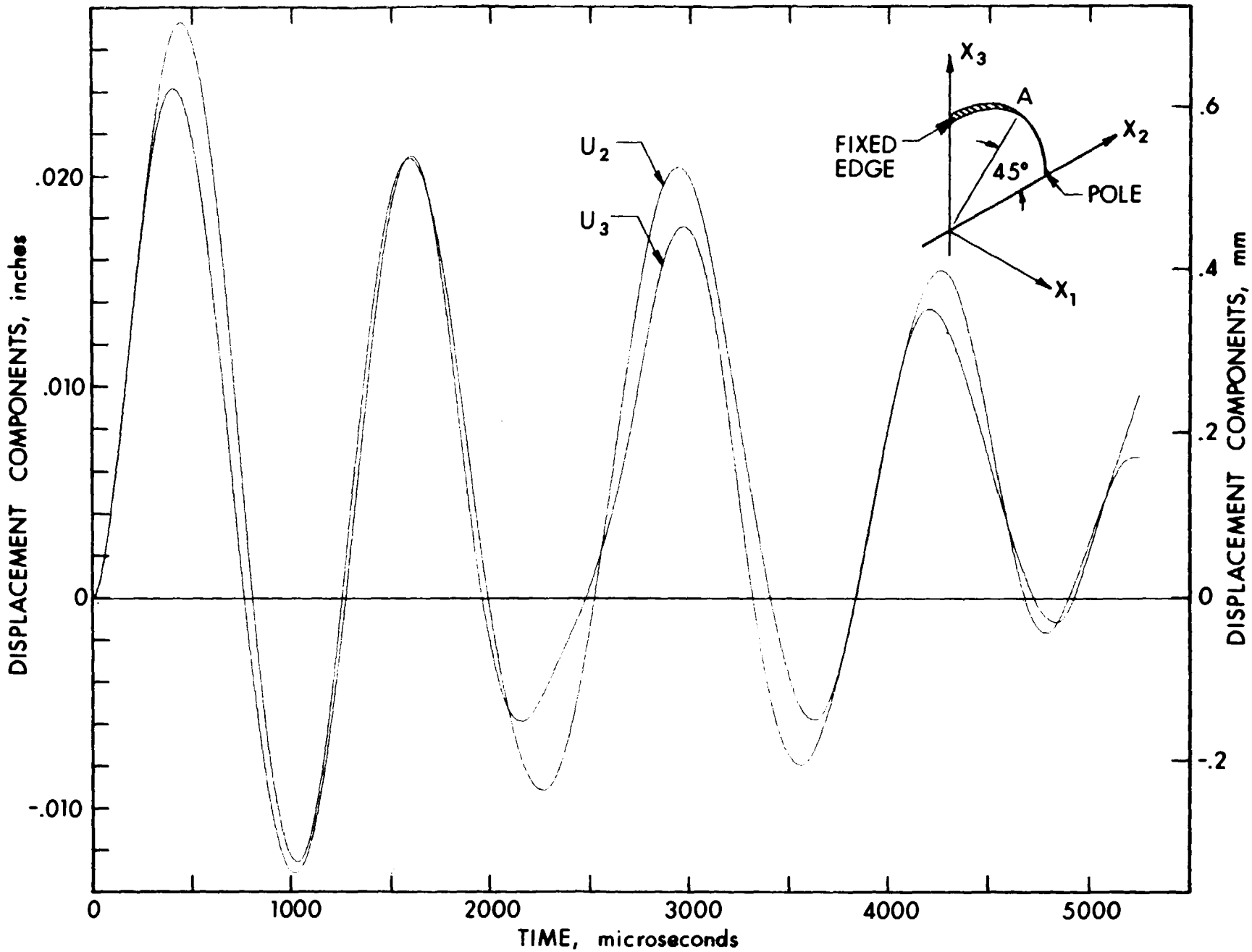

Figure 4. Transient Displacement Components at Point A, R=5 Feet

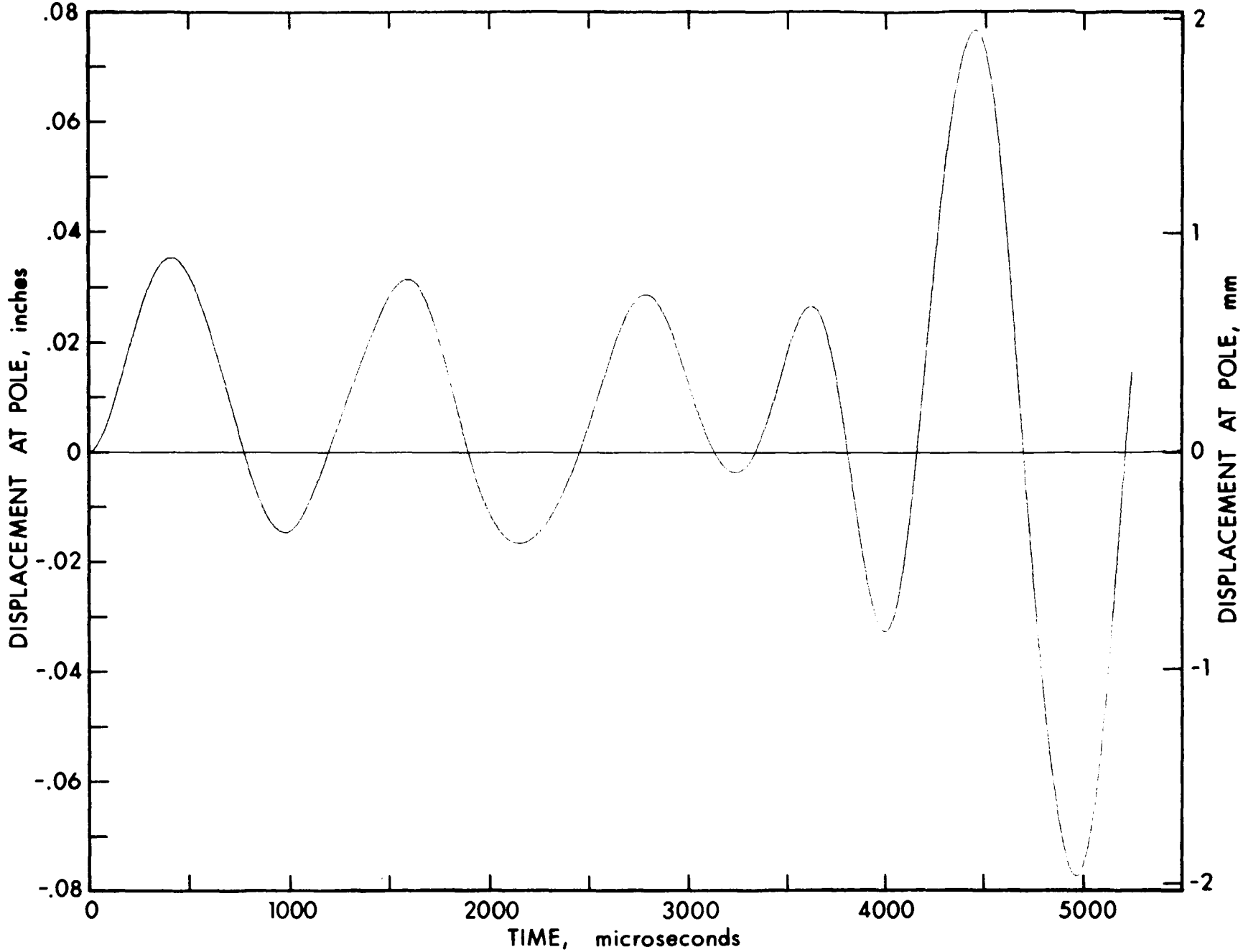

Figure 5. Transient Displacement at Pole of Hemisphere

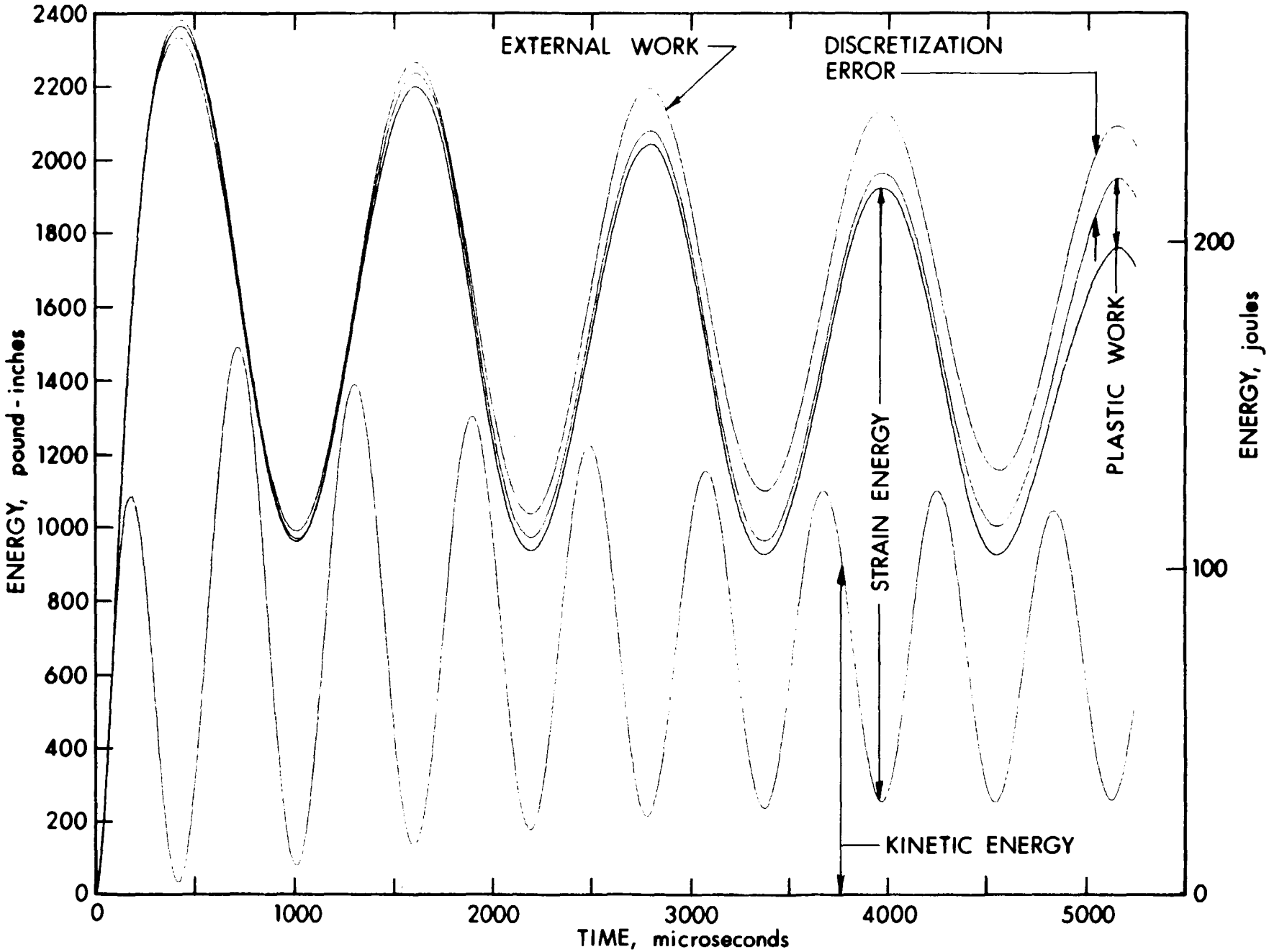

Figure 6. Energy Balance Diagram, R=5 Feet

of the containment structure is already inconveniently small for necessary machinery and service personnel further reductions in R were not pursued. The total weight of the containment structure for R = 5 feet (1.52 m) was determined to be approximately 7000 pounds (31137N), or about 14% of the weight of the corresponding suppressive structure of Reference 2. In this comparison, allowance was made for the weight of flange material required at the boundary of the hemisphere but not for extra weight associated with access provisions, welds, or foundations since these considerations are common to both types of construction. Since the cost of monocoque construction employed for the total containment structure should be considerably less than the cost of fabricating the panel arrays used in the suppressive structure, a comparison on a cost basis should be even more favorable to the containment structure.

Up to this point no consideration has been given to the possibility that fragment-induced damage to a monocoque shell might result in catastrophic rupture when the blast loading is applied. One should estimate the material removal produced by the worst-threat fragment and perform a local three-dimensional analysis using the PETROS 3.5 predicted transient stress field to determine whether a crack would be propagated under such loading. This rather difficult problem in fracture mechanics can be at least partially circumvented by a conservative selection of wall thickness for the monocoque shell (even a doubling of the wall thickness would leave the containment structure in a very favorable competitive position in comparison to a suppressive structure, as may be inferred from the preceding example). However, the part-way-through damaged shell should be designed to at least sustain the quasi-static residual pressure.

B. Hemicylindrical Configuration

Although the previously considered hemispherical configuration has advantages with respect to optimal stressing of the material it clearly has drawbacks regarding access and the shape of the interior volume afforded. Consequently, consideration was given to analysis of the response of a compromise configuration: specifically, a hemicylinder with closed ends, one-quarter of which is illustrated in Figure 7. While certainly not as efficient from a structural viewpoint,* it is regarded as a closer approximation to a configuration which could be employed for an assembly line operation.

This response problem was also treated using the PETROS 3.5 code for the case h = 1 inch (25.4 mm), R = 5 feet (1.52 m) and a cylinder length L of 10 feet (3.05 m). The weight of this structure would be approximately 10500 pounds (46706N). The same charge, two 81mm mortar rounds, was assumed to be detonated on the axis of the cylinder midway

It would certainly be possible to design a more structurally efficient end closure than a flat plate but other considerations relating to the intended application may indicate a preference for a vertical wall.

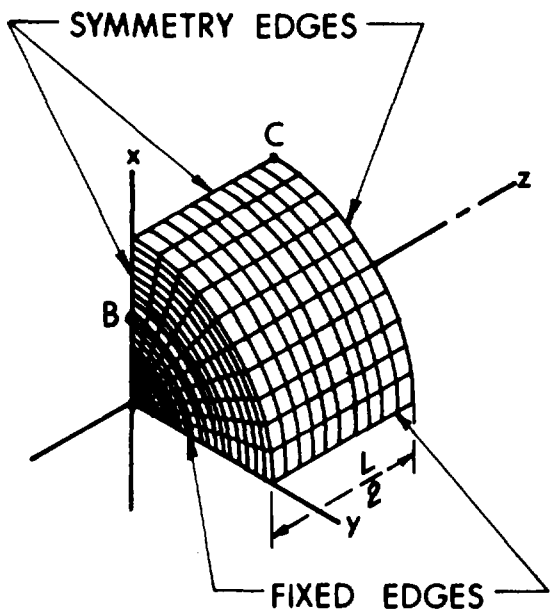

Figure 7. Hemicylinder Geometry, Including Finite Difference Grid

between the ends. The peak reflected pressure on the cylinder at z = L/2 and on the end plates on the cylinder axis is 1000 psi (6.89 MPa) as for the hemisphere. At other locations the peak pressure is less due to spherical divergence of the blast wave and oblique reflection. Empirical data on this pressure were fitted by a quadratic approximation in the response calculations. The pressure at each location was then assumed to decay exponentially until the equilibrium pressure (100 psi (0.69MPa)) is reached, which is less than for the hemisphere due to the greater internal volume.

The deflections at B and C (Figure 7) are the greatest for the end plate and the hemicylinder, respectively. At both locations the maximum deflections exceed those for the hemisphere, which is in agreement with expectations since the deformation of the hemicylinder is highly inhomogeneous. While strains at certain points are greater than for the hemisphere, these are very much less than those required to produce rupture so the structure should still be able to contain the explosion.

III. CONCLUDING REMARKS

It has been demonstrated, through use of a rather complete and rigorous nonlinear shell response methodology, that it is possible to design a containment structure that is significantly lighter and less complex to fabricate than a suppressive structure of corresponding capability.

An examination of the characteristics of the near-optimal hemispherical structure permits the identification of factors which contribute to efficiency of protective structures:

1. Shapes which promote the development of membrane restoring forces before large deformations occur are desirable in order that the entire volume of structural material experiences significant plastic work. Flat plates and straight beams supported at the edges which resist deformation principally by nonuniformly distributed bending stresses are notoriously inefficient.

2. Since structural weight of fragment containment structures varies approximately as the midsurface area, the structure should be made as small as the requirement of blast survivability permits. However, it is recognized that considerations of internal volume required for necessary machinery and for service personnel may dictate the use of a somewhat larger, less efficient structure.

3. While the use of vented spaced plates may be desirable from the viewpoint of blast and fragment suppression, in configurations where significant bending cannot be avoided (as in box-type structures) the use of multiple plates with no shear ties is less efficient than a single plate of the same total thickness.

In comparing suppressive structures with those designed for total containment it was believed that the ventilated structure might be somewhat lighter because it does not have to resist the full blast loading. Conversely, it was recognized that stress concentrations associated with openings in the ventilated structure would require added weight so that the net effect could not be determined a priori. However, the apparent greater weight of "equivalent" suppressive structures (aside from that part due to greater size) would indicate that either the stress concentration effect is dominant or designers have not been able to take advantage of the reduced blast loading due to uncertainty as to its extent. Further, it appears from examinations of calculations that structures which have been designed to survive the initial portion of a blast load such as depicted in Figure 2 can withstand the much lower equilibrium pressure indefinitely, thus obviating the need for rapid venting of the confined pressure.

The writers prefer to leave for future judgment any determination as to whether suppressive structures can be designed to be competitive with total containment structures from an engineering viewpoint. However, considerable research and methodology development in the areas of blast dissipation, structural component loading, and structural response of complex configurations will be required before rational design of suppressive structures can be performed with the same degree of confidence as presently exists for containment structures. Perhaps some combination of these concepts will eventually prove most satisfactory for practical applications. Figure 8 illustrates such a compromise which may be useful for an assembly line operation. Munitions on pallets are brought by conveyor belt to and away from a station where a hazardous operation is performed. This station is enclosed in a containment structure which has openings for the conveyor belt and pallets at each end. Suppressive panels to cover the openings required for pallets as well as deflectors to divert residual blast upwards would be raised and lowered hydraulically to permit passage of pallets. In the closed position the ends of the suppressive panel would be nested in wedge supports capable of resisting any loads produced by an accidental detonation. While not necessary, additional suppressive panels could be located in the upper portion of the cylindrical structure to provide controlled upward directed venting of the explosion products.

Subsequent to the completion of the study reported herein the authors became aware of the extensive investigation which had been performed by BRL for the Atomic Energy Commission concerning the safety of outer containment structures for nuclear reactors. The results of this investigation (References 4 - 10)* serve to corroborate the conclusion of this report that monocoque structural shells composed of spherical or cylindrical segments are desirable and efficient configurations for containment of accidental explosions.

**References 4 - 10 are listed on page 20.*

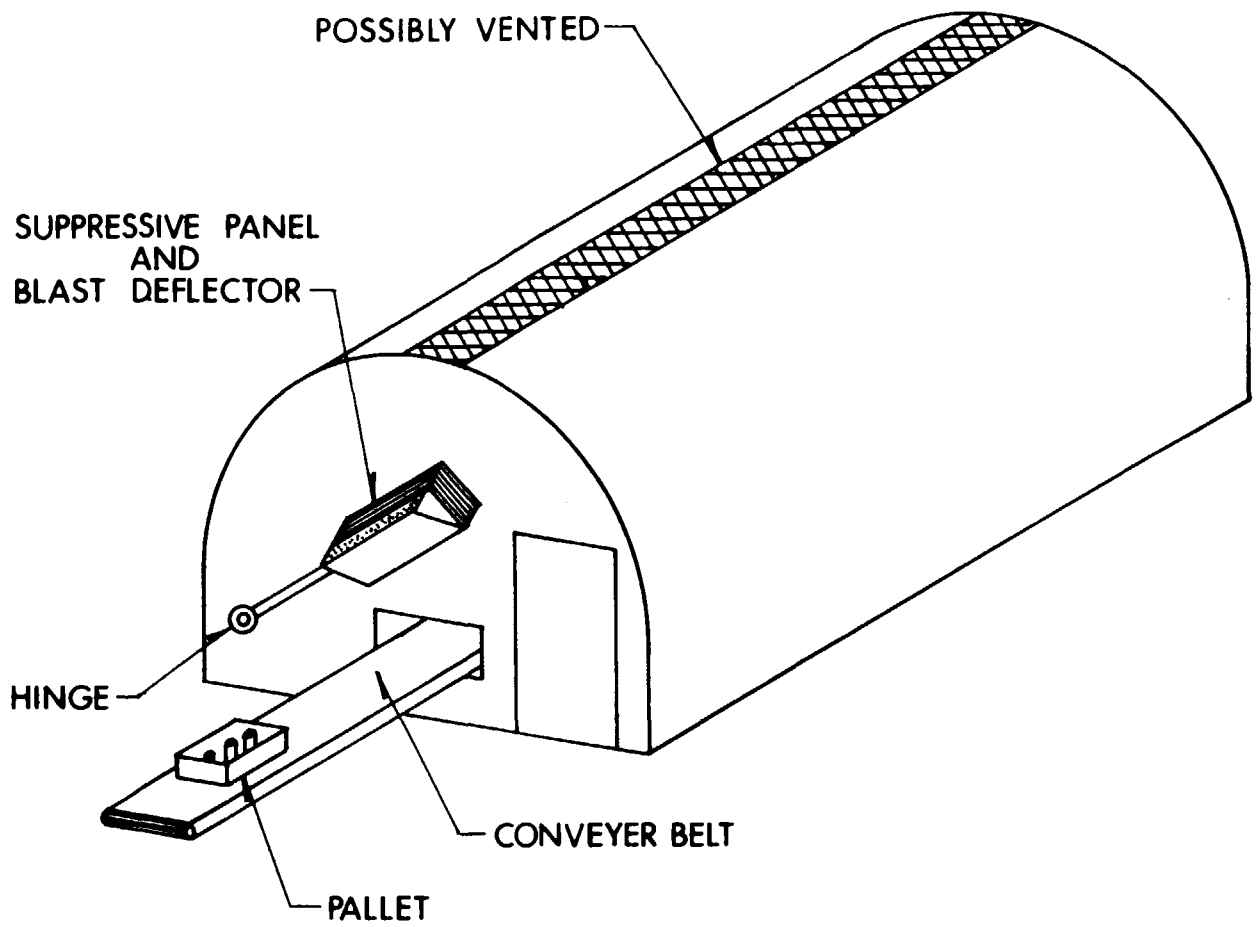

Figure 8. Protective Structure Concept for Assembly Line

REFERENCES

1. S. D. Pirotin, B. A. Berg, and E. A. Witner, "PETROS 3.5: New Developments and Program Manual for the Finite-Difference Calculation of Large Elastic-Plastic Transient Deformations of Multilayer Variable-Thickness Shells," U.S. Army Ballistic Research Laboratories Contract Report No. 211, February 1975. AD# A007215.

2. "Design, Fabrication and Test of a Suppressive Structure for Application to an 81mm Mortar Round Automated Assembly Facility," Draft Report, Edgewood Arsenal Resident Office, National Aeronautics and Space Administration, Bay St. Louis, MS, 9 January 1974.

3. B. Bertrand, C. Brown, D. Dunn, N. Huffington, J. Kineke, C. Kingery, R. Meissner, A. Ricchiazzi, S. Robertson, and R. Vitali, "Suppressive Structures - A Quick Look," BRL Interim Memorandum Report No. 190, February 1974.

4. W. E. Baker, and F. J. Allen, "The Response of Elastic Spherical Shells to Spherically Symmetric Internal Blast Loading," BRL Memorandum Report No. 1113, November 1957. AD# 156639.

5. W. E. Baker, W. O. Ewing, Jr., and J. W. Hanna, "Laws For Large Elastic Response and Permanent Deformation of Model Structures Subjected to Blast Loading," BRL Report No. 1060, December 1958. AD# 213918.

6. J. W. Hanna, W. O. Ewing, Jr., and W. E. Baker, "The Elastic Response to Internal Blast Loading of Models of Outer Containment Structures For Nuclear Reactors," BRL Report No. 1067, February 1959. AD# 217257.

7. W. E. Baker, "The Elastic-Plastic Response of Thin Spherical Shells to Internal Blast Loading," BRL Memorandum Report No. 1194, February 1959. AD# 217256.

8. J. W. Hanna, W. O. Ewing, Jr., "Effectiveness of Lining Materials in Increasing The Blast Resistance of a Simulated Outer Containment Vessel for a Nuclear Reactor," BRL Memorandum Report No. 1341, April 1961. AD# 259902.

9. W. E. Baker, "The Elastic Response of Thin Spherical Shells to Internal Blast From Eccentrically Placed Explosive Charges," BRL Memorandum Report No. 1520, November 1963. AD# 428286.

10. J. W. Hanna, and W. O. Ewing, Jr., "The Plastic Response to Internal Blast Loading of Models of Outer Containment Structures for Nuclear Reactors," BRL Memorandum Report No. 1530, January 1964. AD# 433618.

A1. H. Kolsky, "Stress Waves in Solids," Oxford, 1953.

APPENDIX

RESULTS OF THE EXTENDED SOLUTION

The growth of displacement at the pole near the end of the previously discussed solution (see Figure 5) and the evidence in Figure 6 that the plastic work was still increasing gave rise to concern that this solution might be numerically unstable and thus invalid. This concern was dispelled when results for a much longer (in time) solution of the same problem were obtained. The PETROS 3.5 code was run for 3050 cycles (22875 microseconds) in an undamped mode, after which artificial damping was introduced to suppress the elastic oscillations. The solution self-terminated at cycle 3173 (23797.5 microseconds) when a criterion for per cent reduction of kinetic energy was satisfied. This extended solution provides insights into several aspects of the response which were not apparent in the abbreviated solution.

The displacement components at point A (which are representative of points not adjacent to the boundary or to the pole), previously shown in Figure 4, are presented in Figure A-1 for the extended solution. It may be seen that the first peak does correspond to the maximum deflection at this point. The subsequent oscillations have a positive bias, principally due to the residual internal pressure. The predicted displacement at point A after oscillations are damped out is 0.0063 inches (0.160 mm) which is almost exactly the deflection of an elastic sphere under the residual pressure. Therefore, it can be inferred that the permanent deflection at this location after the pressure is removed would be extremely small.

The extended solution for the displacement at the pole is shown in Figure A-2. The growth in amplitude noted in Figure 5 continues in an oscillatory manner, reaching a maximum of 0.136 inches (3.45 mm) at about 8000 microseconds. This displacement is less than 14% of the thickness of the shell so it may be concluded that geometric nonlinearities are not significant in this problem. Initially the pole moves in the same manner as the typical internal point A but by around 3000 microseconds the motion of the neighborhood of the pole is significantly out of phase with that of other points on the shell. The unique behavior of the pole in relation to that of the remainder of the shell can be better visualized by study of the series of deformed meridional contours shown in Figure A-3.

Were it not for the fixed boundary this centrally loaded hemisphere would respond exclusively in a spherically symmetric breathing mode. The effect of the boundary is introduced through flexural waves which initiate at the boundary and propagate towards the pole. In discussing wave propagation in a shell one must distinguish between (a) the physical behavior of the real or perfectly modeled shell and (b) the behavior predicted by the mathematical model actually employed. For (a) we know that flexural wave velocities in elastic media depend upon the

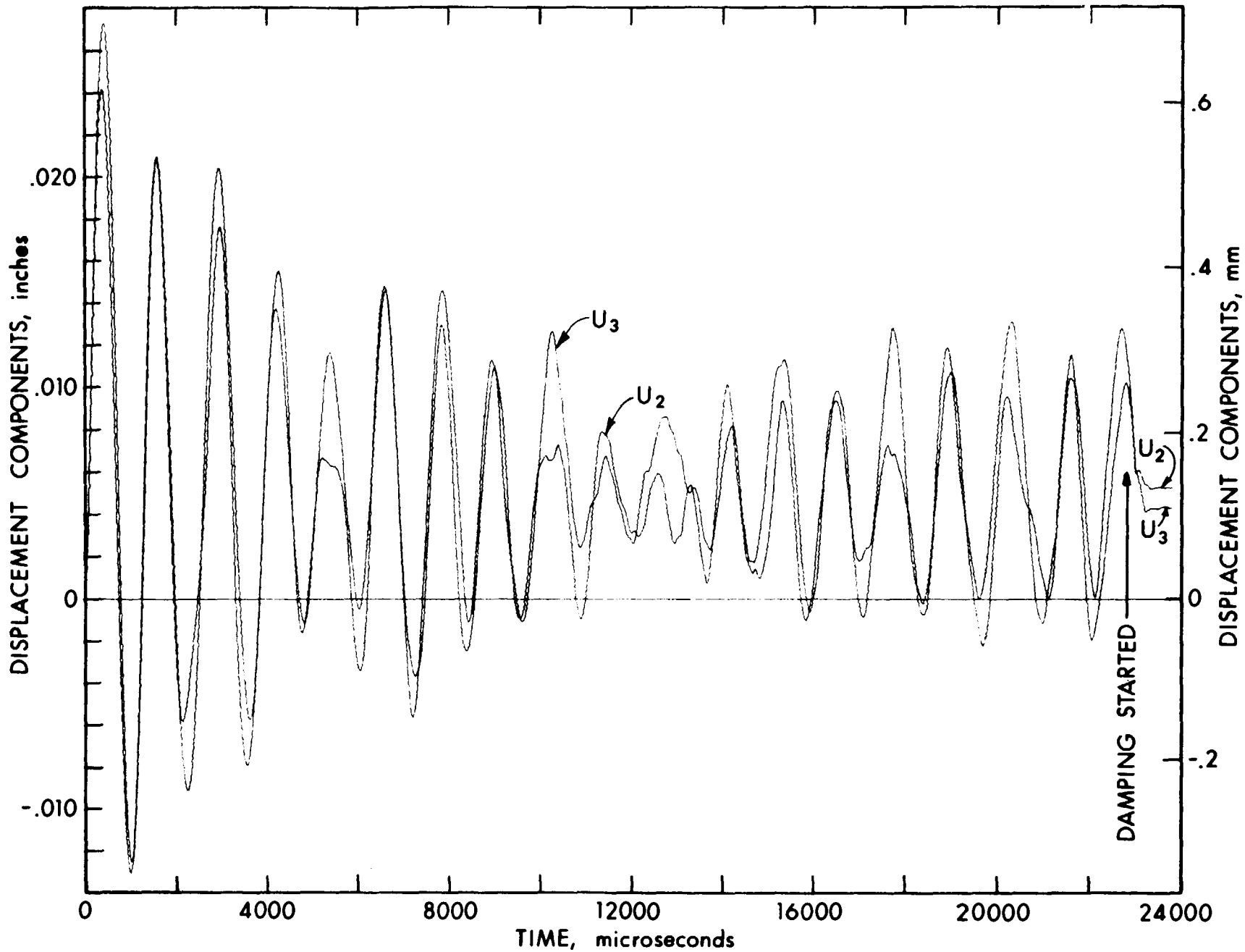

Figure A-1. Transient Displacement Components at Point A (Extended Solution)

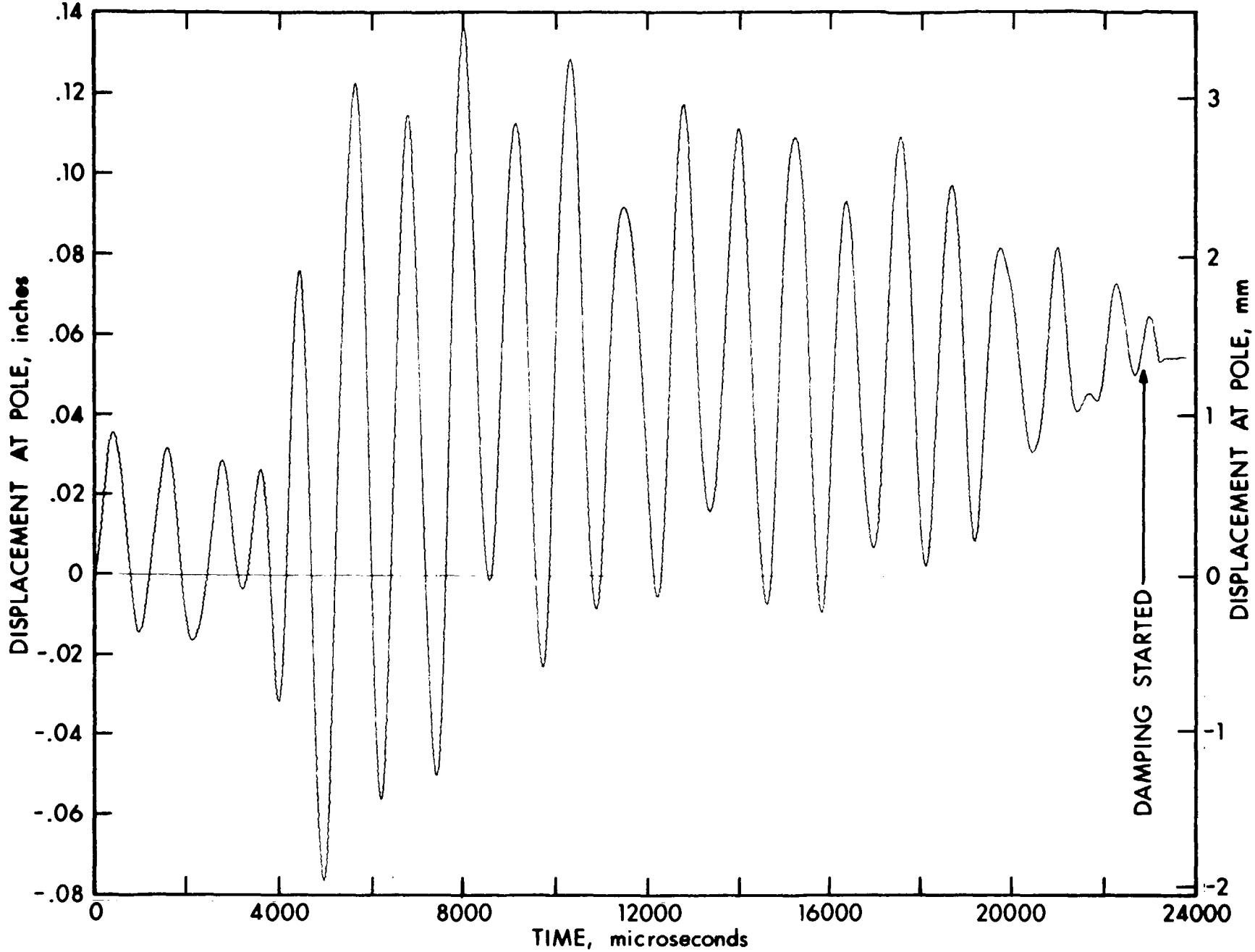

Figure A-2. Transient Displacement at Pole (Extended Solution)

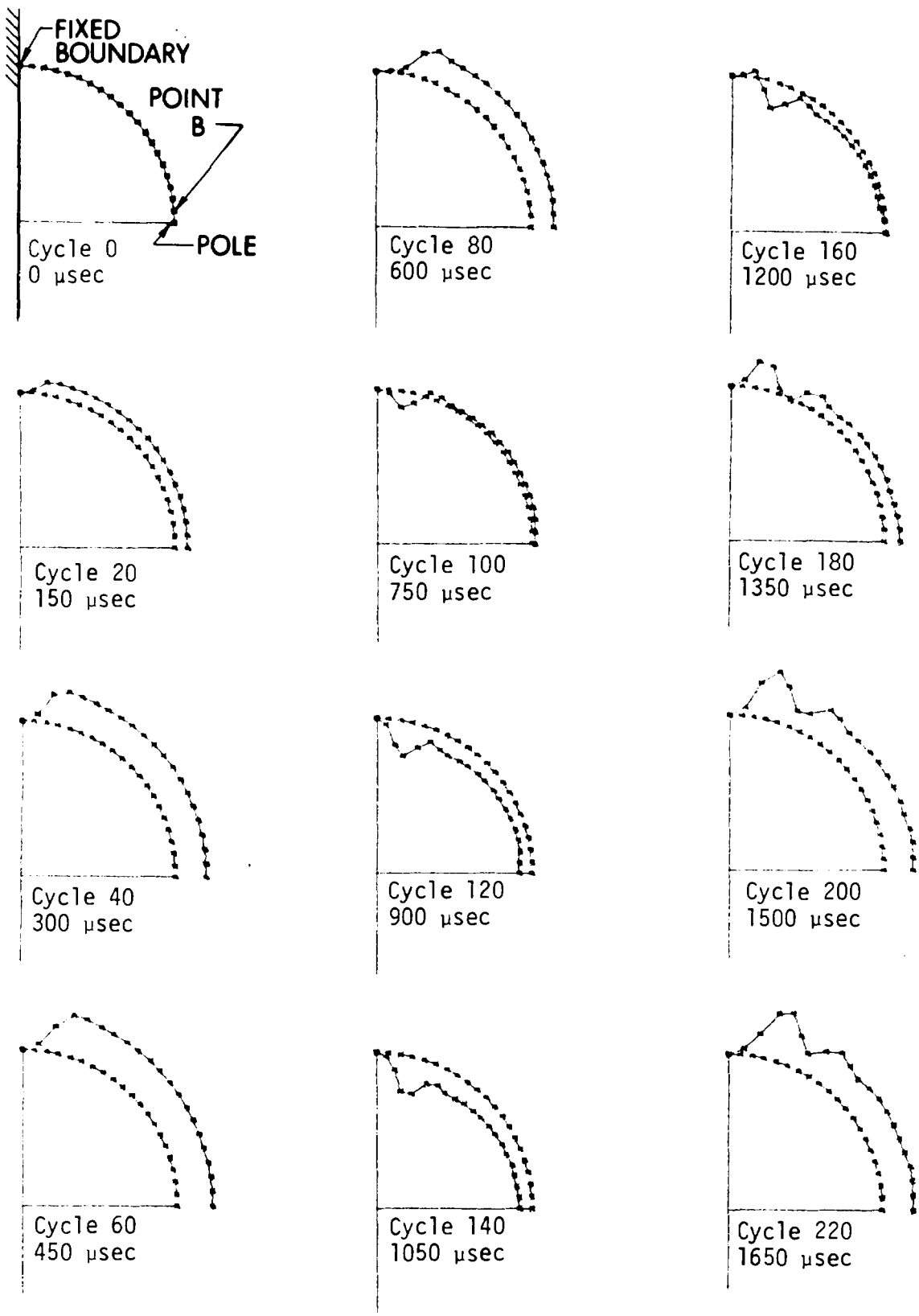

Figure A-3. Meridional Deformation Modes

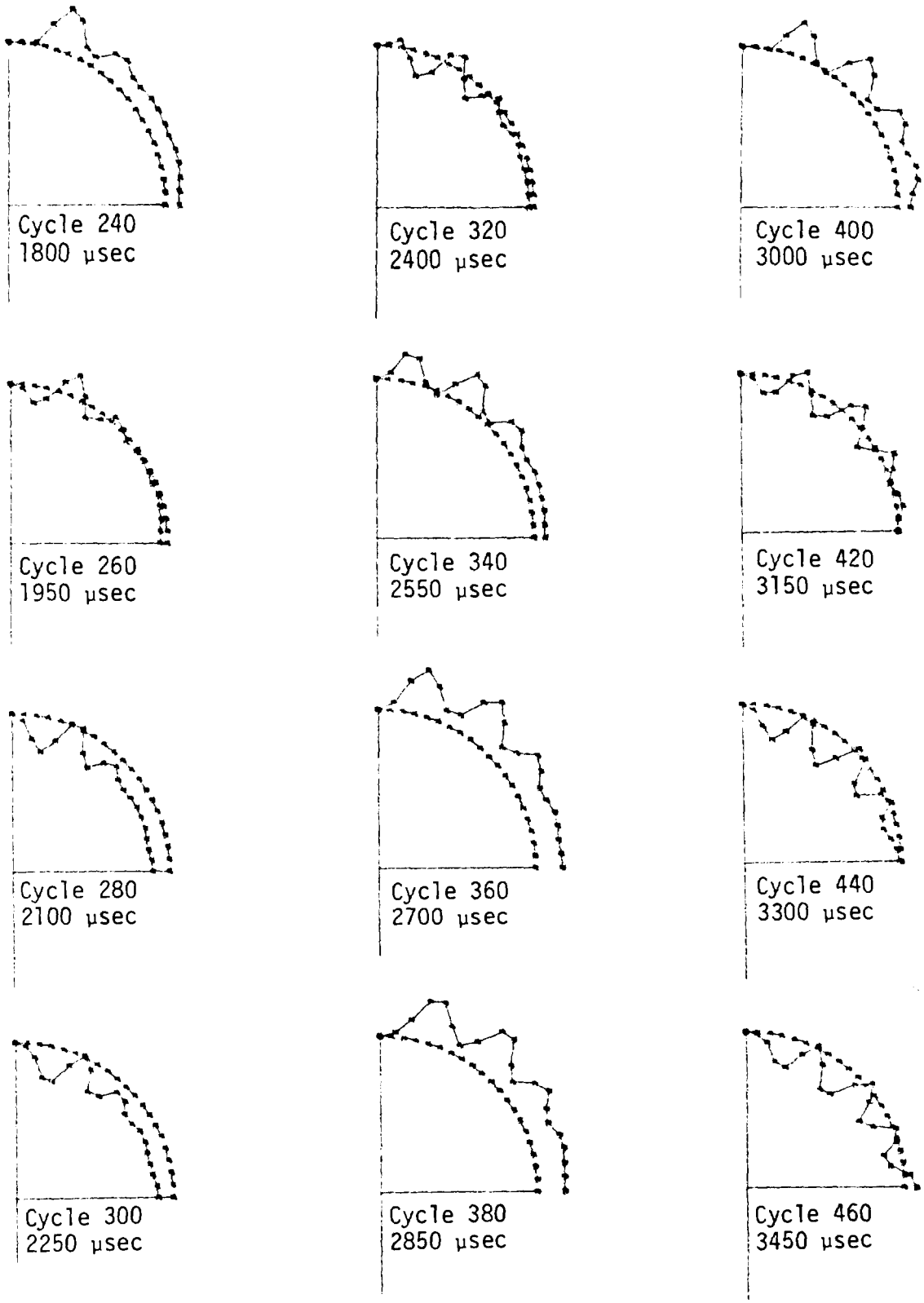

Figure A-3. (Continued)

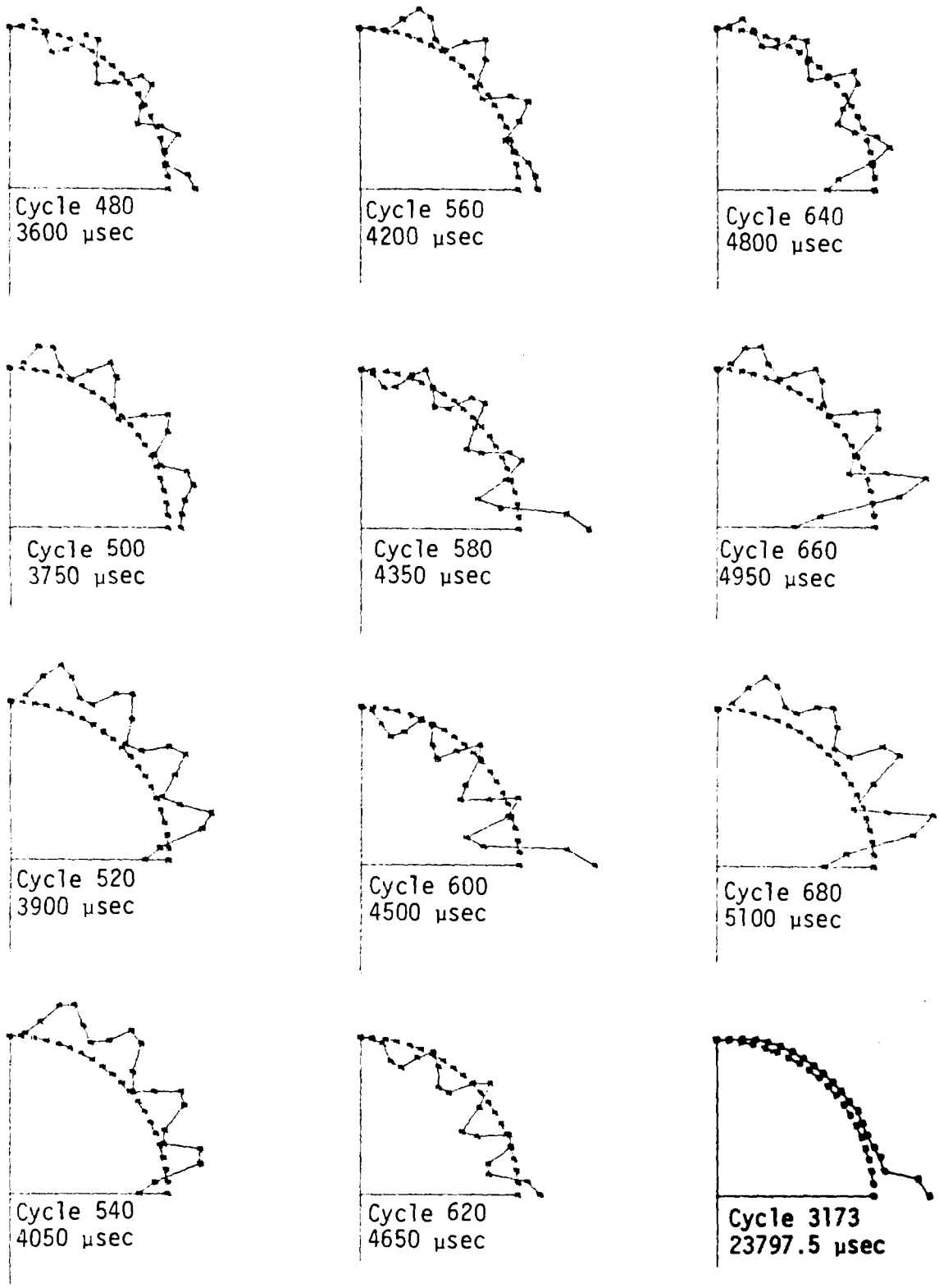

Figure A-3. (Concluded)

wave length λ (i.e., flexural waves are dispersive). For the material properties and geometric parameters of the case under consideration these wave speeds and the times t_a required for a disturbance to travel from the boundary to the pole are as follows:

Limiting Cases	Wave Speed in/sec	Wave Speed m/sec	t_a microseconds
Long Waves ($\lambda >> h$)	1005	25.5	93800
Short Waves ($\lambda \to o$)	117600	2987.0	802

where h is the shell thickness. The short wave length limit corresponds to the velocity of Rayleigh surface waves while the phase velocity for long waves is given by $c = 378700/\lambda$ (in/sec). Since the bounds on t_a are so widely separated, it is small comfort that the actual time at which the pole displacement experiences rapid growth falls within these limits. For (b) we are using a Kirchhoff shell theory which neglects transverse shear deformation and rotatory inertia. Such theories have the defect that they predict unbounded wave speeds as $\lambda \to 0$. This does not necessarily entail the prediction that finite disturbances will arrive prematurely at positions away from the source, however, since the spurious precursor may have only infinitesimal amplitude. When the shell equations are solved by the finite difference method (as is done by PETROS 3.5) another complication arises. In this case the possible propagation speed is finite, being limited to two mesh spaces per time cycle. On this basis a disturbance originating at the boundary could reach the pole by Cycle 10 (75 microseconds) for the mesh employed, which is much sooner than the minimum theoretical t_a. However, it may be seen from the plot for Cycle 20, Figure A-3, that there is no appreciable deviation from sphericity except in the immediate neighborhood of the boundary. Consequently, the possible spurious precursor is truly insignificant for this problem.

By examination of Figure A-3 one sees that each full oscillation of the breathing mode initiates a flexural wave which travels toward the pole. While this wave is dispersive (as evidenced by its decay in amplitude at its leading edge) the principle component may be regarded as being a sinusoidal wave whose wave length is $\lambda = c\tau$ (where τ is the period of the breathing oscillations and c is the phase velocity for long flexural waves). From Figure 4 the period τ may be determined to be approximately 1400 microseconds. Using this value and the previous expression for the phase velocity leads to $\lambda = 23.03$ inches (0.585 m) which is in good agreement with the modes exhibited in Figure A-3. To determine the rate at which the energy of flexural vibrations is propagated it is necessary to determine the group velocity (Reference A-1). For long waves this is found to be twice the phase velocity, i.e., $c_g = 757400/\lambda$ inches/sec. Then the time of arrival for significant

A-1 *H. Kolsky, "Stress Waves in Solids," Oxford, 1953.*

flexural energy at the pole is around 2866 microseconds which appears to coincide with the time at which a significant phase difference between the motions of point A and the pole develops. It should be emphasized that, since this problem is axisymmetric, there is an effect of focusing of flexural vibratory energy at the pole, with continued reinforcement as subsequent waves arrive. On this basis the larger response at the pole appears quite reasonable. Figure A-3 also shows the meridional profile at Cycle 3173 (after all oscillations have been suppressed by damping but internal pressure is still applied. By subtracting the static elastic displacement produced by this pressure one arrives at the estimate that the final deformed state of the hemisphere will entail a "pimple" at the pole which is 0.048 inches (1.22 mm) high.

Transient strain components on the outer and inner surfaces of the hemisphere at point B (see Cycle 0, Figure A-3) are plotted in Figure A-4. The strains on the inner and outer surfaces are initially in phase and of equal value; i.e., they are membrane strains corresponding to the breathing mode. At around 3000 microseconds the strain components on the two surfaces become appreciably out of phase and of unequal magnitude, signaling the buildup of the flexural deformation previously discussed. As the total strains increase in amplitude the circumferential and meridional components on the same surface become unequal due to disparity in plastic straining in the two orthogonal directions (which is possible since point B is not at the pole).

The energy diagram comparable to Figure 6 but for the extended solution is presented as Figure A-5(a). One sees that the double frequency for the kinetic energy persists even after the excitation of bending modes becomes significantly large. The numerical solution is obviously stable, at least for the response duration of interest. The discretization error, defined as: Discretization Error = External Work - (Kinetic Energy + Strain Energy + Plastic Work) does not continue to grow but slowly oscillates in amplitude. After damping is introduced the ordinate between curves 3 and 4 of Figure A-5(a) becomes the sum of the damping work and the discretization error (principally the former). The growth of the plastic work is displayed separately in Figure A-5(b), which makes apparent the irreversible nature of this quantity. One sees that the plastic work approaches a limit in an asymptotic manner but not until near the end of the extended solution. Introduction of damping obviously has no effect on the plastic work (as desired). The small amount of plastic work which occurs before 2000 microseconds was localized near the fixed boundary. The stepwise growth of plastic work after 4000 microseconds correlates exactly with the large amplitude excursions of bending strains depicted in Figure A-4, confirming that the bulk of the plastic deformation takes place in the immediate neighborhood of the pole.

Although the results for the extended solution which have been discussed in this Appendix have made apparent several features of the response of the hemispherical shell which were not deducible from the abbreviated solution presented in the body of this report, no alteration in the

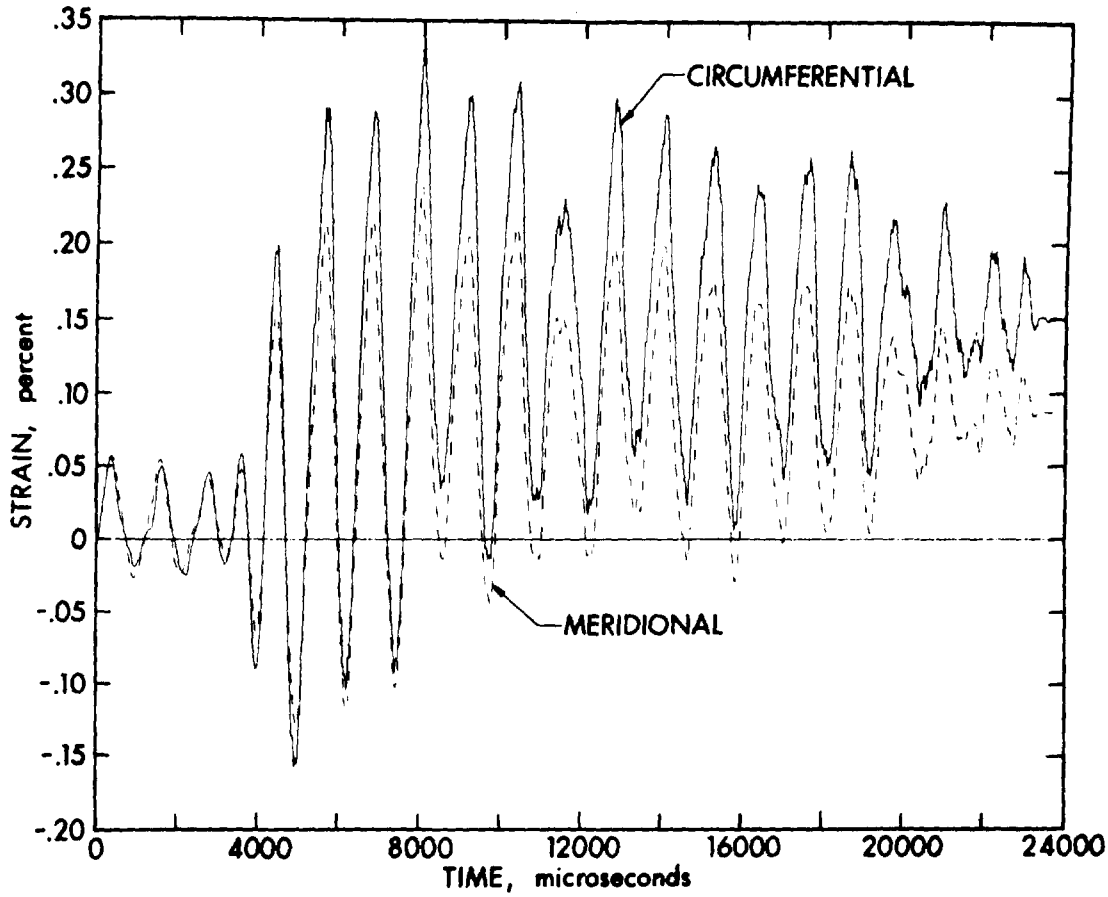

(a) Outer Surface Strain Components

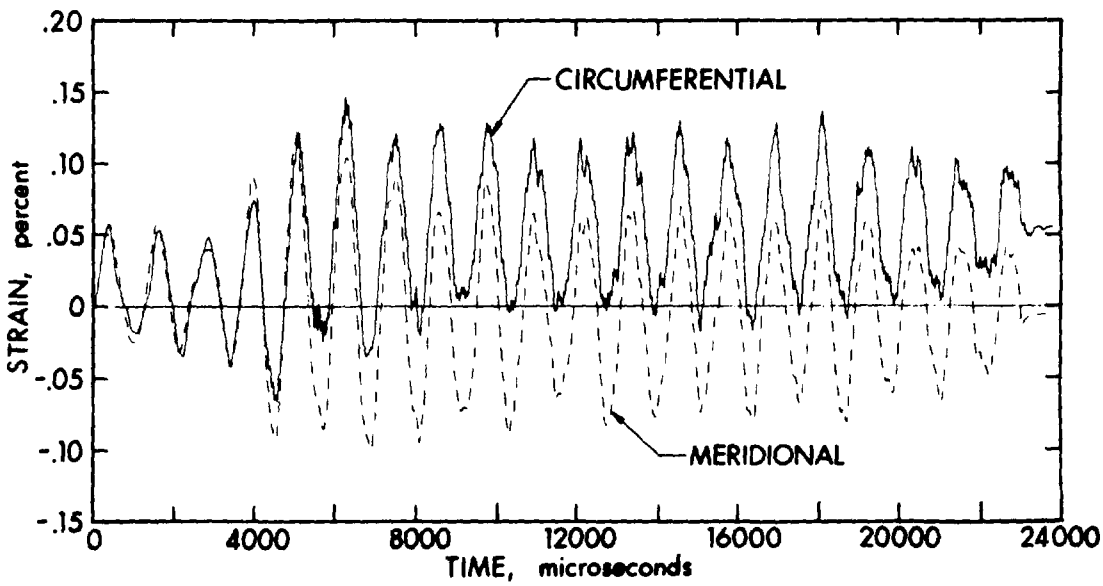

(b) Inner Surface Strain Components

Figure A-4. Surface Strains at Point B

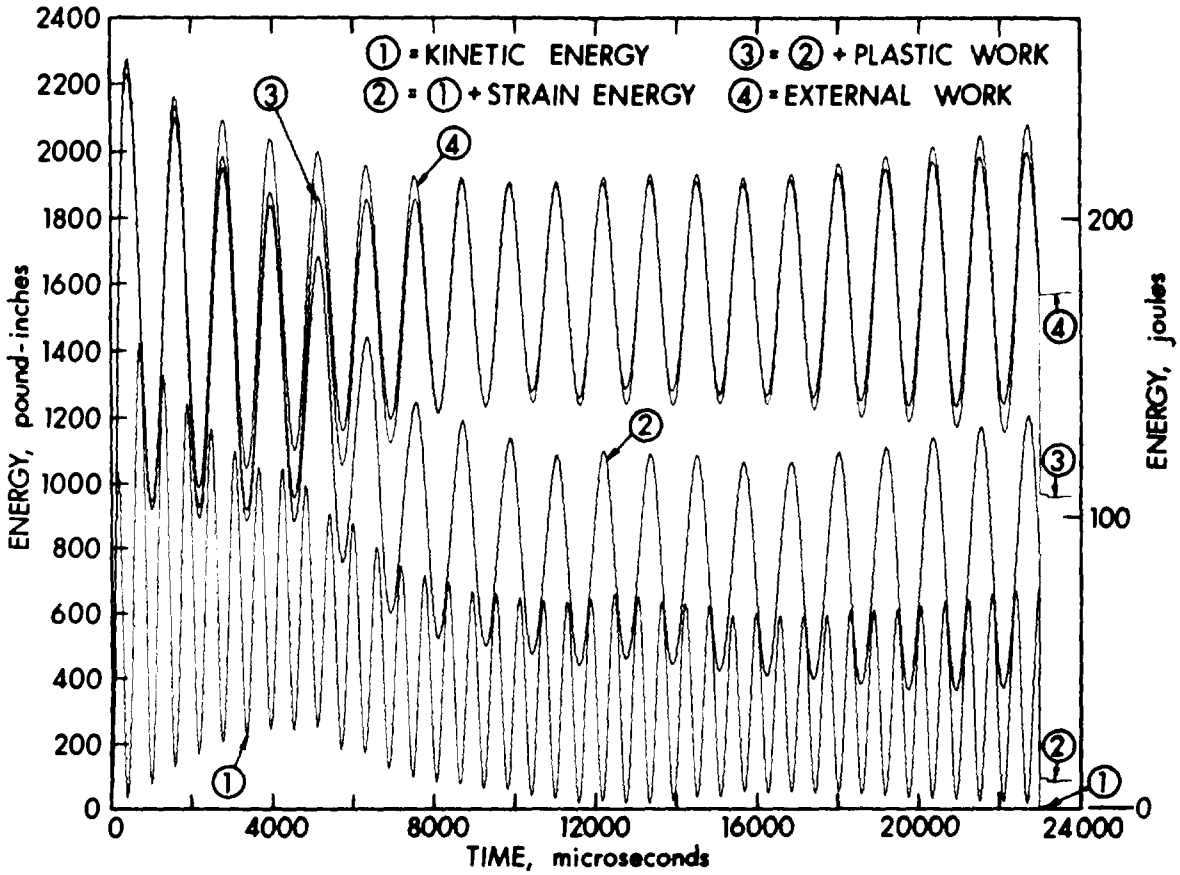

(a)

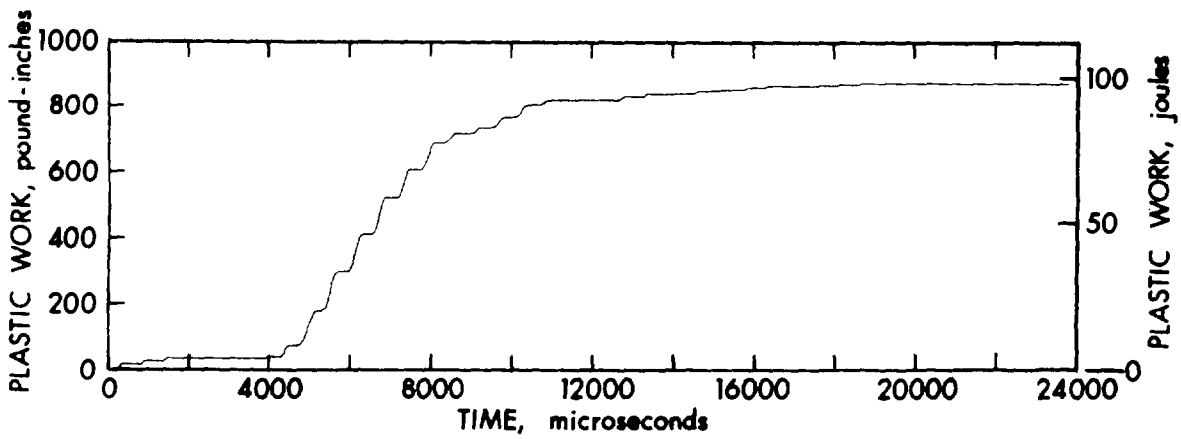

(b)

Figure A-5. Energy/Work Diagrams (Extended Solution)

conclusions regarding the ability of the 5 foot (1.52 m) radius hemisphere to contain the prescribed blast loading is required.

DISTRIBUTION LIST

No. of Copies	Organization
12	Commander Defense Documentation Center ATTN: DDC-TCA Cameron Station Alexandria, VA 22314
1	Office Secretary of Defense Office, DDR&E ATTN: Mr. J. Persh, Staff Specialist Materials and Structures Washington, DC 20301
1	Director Defense Advanced Research Projects Agency 1400 Wilson Boulevard Arlington, VA 22209
1	Director Weapons Systems Evaluation Group ATTN: CPT Donald E. McCoy Washington, DC 20305
3	Director Institute for Defense Analysis ATTN: Dr. J. Menkes Dr. J. Bengston Tech Info Ofc 400 Army-Navy Drive Arlington, VA 22202
1	Assistant to the Secretary of Defense (Atomic Energy) ATTN: Document Control Washington, DC 20301
2	Director Defense Nuclear Agency ATTN: Mr. J. F. Moulton, SPAS Dr. E. Sevin, SPSS Washington, DC 20305
4	Director Defense Nuclear Agency ATTN: SPTL Tech Lib (2 cys) APSI (ARCHIVES) STSP Washington, DC 20305
1	Commander Field Command Defense Nuclear Agency ATTN: Tech Lib, FCWS-SC Kirtland AFB, NM 87115
1	Chief Las Vegas Liaison Office Field Command TD, DNA ATTN: Document Control P.O. Box 2702 Las Vegas, NV 89104
1	DNA Information and Analysis Center TEMPO, General Electric Co. Center for Advanced Studies ATTN: DASIAC 816 State Street Santa Barbara, CA 93102
1	Director Defense Communications Agency ATTN: NMCSSC (Code 510) Washington, DC 20305
2	Director Defense Intelligence Agency ATTN: DT-1C, Dr. J. Vorona DT-2 Washington, DC 20301
2	Chairman Joint Chiefs of Staff ATTN: J-3, Operations J-5, Plans & Policy (R&D Division) Washington, DC 20301

DISTRIBUTION LIST

No. of Copies	Organization
1	Commander US Army Materiel Development and Readiness Command ATTN: DRCDMA-ST 5001 Eisenhower Avenue Alexandria, VA 22333
2	Commander US Army Materiel Development and Readiness Command ATTN: DRCDE-WB DRCDE-W, Mr. J. Corrigan 5001 Eisenhower Avenue Alexandria, VA 22333
1	Commander US Army Materiel Development and Readiness Command ATTN: DRCPM-CS 5001 Eisenhower Avenue Alexandria, VA 22333
1	Commander US Army Aviation Systems Command ATTN: DRSAV-E 12th and Spruce Streets St. Louis, MO 63166
1	Director US Army Air Mobility Research and Development Laboratory Ames Research Center Moffett Field, CA 94035
1	Commander US Army Electronics Command ATTN: DRSEL-RD Fort Monmouth, NJ 07703
3	Commander US Army Missile Command ATTN: DRSMI-R DRSMI-AOM, Library DRSMI-RSS, Mr. B. Cobb Redstone Arsenal, AL 35809
2	Commander US Army Missile Command ATTN: DRSMI-RX, Mr. W. Thomas DRSMI-RR, Mr. L. Lively Redstone Arsenal, AL 35809
1	Commander US Army Tank Automotive Logistics Command ATTN: DRSTA-RHFL Warren, MI 48090
2	Commander US Army Mobility Equipment Research & Development Command ATTN: Tech Docu Cen, Bldg 315 DRSME-RZT Fort Belvoir, VA 22060
3	Commander US Army Armament Command ATTN: DRSAR-RDT; DRSAR-RDN DRSAR-MT Rock Island, IL 61202
1	Commander US Army Frankford Arsenal ATTN: SARFA-L6100, Dr. P. Flynn Philadelphia, PA 19137
3	Commander US Army Picatinny Arsenal ATTN: SARPA-V Mr. G. Demitrack Mr. M. Weinstein SARPA-MT-F Mr. John Canavan Dover, NJ 07801
1	Commander US Army Rock Island Arsenal Rock Island, IL 61202
1	Commander Dugway Proving Ground ATTN: STEDP-TO-H (Mr. Miller) Dugway, UT 84022

DISTRIBUTION LIST

No. of Copies	Organization
1	Commander US Army Watervliet Arsenal Watervliet, NY 12189
1	Commander US Army Harry Diamond Laboratories ATTN: DRXDO-TI 2800 Powder Mill Road Adelphi, MD 20783
1	Commander US Army Materials and Mechanics Research Center ATTN: DRXMR-ATL Watertown, MA 02172
1	Commander US Army Natick Research and Development Command ATTN: DRXRE, Dr. D. Sieling Natick, MA 01762
1	Commander US Army Foreign Science and Technology Center ATTN: Rsch & Data Branch Federal Office Building 220 7th Street, NE Charlottesville, VA 22901
1	Director DARCOM, ITC ATTN: Dr. Chiang Red River Depot Texarkana, TX 75501
1	Commander US Army TRADOC Systems Analysis Activity ATTN: ATAA-SA White Sands Missile Range NM 88002
2	HQDA (DAMA-AR; NCL Div) Washington, DC 20310
1	Director US Army Advanced BMD Technology Center ATTN: M. Whitfield P.O. Box 1500 Huntsville, AL 35807
1	Commander US Army Ballistic Missile Defense Systems Command ATTN: J. Veeneman P.O. Box 1500, West Station Huntsville, AL 35807
1	Commander US Army Research Office P.O. Box 12211 Research Triangle Park NC 27709
1	US Army Engineering Division ATTN: Mr. Char P.O. Box 1600 Huntsville, AL 35809
2	Director Joint Strategic Target Planning Staff ATTN: JLTW JPTP Offutt AFB Omaha, NE 68113
4	Chief of Naval Operations ATTN: OP-03EG OP-97 OP-754 OP-985FZ Department of the Navy Washington, DC 20350
1	Assistant Secretary of the Navy (Research & Development) Navy Department Washington, DC 20350

DISTRIBUTION LIST

No. of Copies	Organization
1	Chief of Naval Material Navy Department ATTN: Code 148, Dr. T. Quinn Arlington, VA 22217
1	Commander David W. Taylor Naval Ship Research & Development Center ATTN: Dr. W. W. Murray, Code 17 Bethesda, MD 20084
2	Commander US Naval Surface Weapons Center ATTN: Mr. J. C. Talley Dr. W. Soper Dahlgren, VA 22448
2	Commander Naval Surface Weapons Center ATTN: Code 241, Mr. Proctor Mr. Kushner Silver Spring, MD 20910
3	Commander US Naval Surface Weapons Center ATTN: Dr. Leon Schindel Dr. Victor Dawson Dr. P. Huang Silver Spring, MD 20910
1	Commander US Naval Weapons Center ATTN: Code 6031 Dr. W. Stronge China Lake, CA 93555
11	Officer in Charge US Naval Weapons Center ATTN: Code P80962 Pasadena Annex 3203 East Foothill Boulevard Pasadena, CA 91107
1	Commander US Naval Ship Research and Development Center Facility ATTN: Mr. Lowell T. Butt Underwater Explosions Research Division Portsmouth, VA 23709
1	Commander US Naval Weapons Evaluation Facility ATTN: Document Control Kirtland AFB Albuquerque, NM 87117
1	Director US Naval Research Laboratory ATTN: Code 2027, Tech Lib Washington, DC 20390
3	Superintendent US Naval Postgraduate School ATTN: Tech Reports Section Code 57, Prof. R. Ball LT COM H. W. Hickman, SMC #1489 Monterey, CA 93940
1	HQ USAF (AFNIE-CA) Washington, DC 20330
4	HQ USAF (AFRDQ: AFRDOSM; AFRDPM; AFRD) Washington, DC 20330
1	AFSC (DSCPSL) Andrews AFB Washington, DC 20331
2	AFATL (ATRD, R. Brandt) Eglin AFB, FL 32542
1	ADTC (ADBPS-12) Eglin AFB, FL 32542

DISTRIBUTION LIST

No. of Copies	Organization
1	USAFTAWC (OA) Eglin AFB, FL 32542
3	AFWL (WLA; WLD; WLRP, LTC H. C. McClammy) Kirtland AFB, NM 87117
1	AFSWC (SWTSX) Kirtland AFB, NM 87117
4	AFWL (SYT, MAJ W. A. Whitaker; SRR; SUL; SR) Kirtland AFB, NM 87117
2	AFFDL (FDTR) (Dr. F. J. Janik, Jr. Dr. R. M. Bader) Wright-Patterson AFB, OH 45433
3	AFML (MAMD, Dr. T. Nicholas; MANC, Mr. D. Schmidt; MAX, Dr. A. M. Lovelace) Wright-Patterson AFB, OH 45433
2	FTD (TDPTN: TDFBD, J. D. Pumphrey) Wright-Patterson AFB, OH 45433
1	Headquarters Energy Research and Development Administration Department of Military Applications Washington, DC 20545
2	National Aeronautics and Space Administration Aerospace Safety Research and Data Institute ATTN: Mr. S. Weiss Mail Stop 6-2 Mr. R. Kemp Mail Stop 6-2 Lewis Research Center Cleveland, OH 44135

No. of Copies	Organization
1	Director National Aeronautics and Space Administration Scientific and Technical Information Facility P.O. Box 8757 Baltimore/Washington International Airport, MD 21240
1	Director NASA, NSTL ATTN: Ch EARL Bay St. Louis, MI 39520
1	Director Lawrence Livermore Laboratory Technical Information Division P.O. Box 808 Livermore, CA 94550
1	Director Los Alamos Scientific Laboratory ATTN: Dr. J. Taylor P.O. Box 1663 Los Alamos, NM 87544
1	Director ATTN: J. Nall P.O. Box 1925 Washington, DC 20505
1	National Academy of Sciences ATTN: Mr. D. G. Groves 2101 Constitution Avenue, NW Washington, DC 20418
1	Aeronautical Research Associates of Princeton, Inc. ATTN: Dr. C. Donaldson 50 Washington Road Princeton, NJ 08540
1	Aerospace Corporation ATTN: Dr. Harris Mayer P.O. Box 95085 Los Angeles, CA 90045

DISTRIBUTION LIST

No. of Copies	Organization
2	AVCO Corporation Structures and Mechanics Dept ATTN: Dr. William Broding Mr. J. Gilmore Wilmington, MA 01887
2	The Boeing Company Aerospace Group ATTN: Dr. Peter Grafton Dr. D. Strome Mail Stop 8C-68 Seattle, WA 98124
1	Dr. J. C. Shang General American Research Div General American Transportation Corp 7449 N. Natchez Avenue Niles, IL 60648
1	J. G. Engineering Research Associates 3831 Menlo Drive Baltimore, MD 21215
2	Kaman-Avidyne ATTN: Dr. N. P. Hobbs Mr. S. Criscione 83 Second Avenue Northwest Industrial Park Burlington, MA 01803
3	Kaman Sciences Corporation ATTN: Dr. F. H. Shelton Dr. D. Sachs Dr. R. Keefe 1500 Garden of the Gods Road Colorado Springs, CO 80907
1	Knolls Atomic Power Lab ATTN: Dr. R. A. Powell Schenectady, NY 12309
2	Martin Marietta Laboratories ATTN: Dr. P. F. Jordan Mr. R. Goldman 1450 S. Rolling Road Baltimore, MD 21227
1	McDonnell Douglas Astronautics Western Division ATTN: Mr. Samuel D. Mihara 3000 Ocean Park Boulevard Santa Monica, CA 90406
1	Physics International ATTN: Dr. G. Richard Fowles San Leandro, CA 94577
1	R&D Associates ATTN: Dr. Albert L. Latter P.O. Box 9695 Marina del Rey, CA 90291
2	Sandia Laboratories ATTN: Infor Distr Division Dr. W. A. von Riesemann Albuquerque, NM 87115
2	Battelle Columbus Laboratories ATTN: Dr. L. E. Hulbert Mr. J. E. Backofen, Jr. 505 King Avenue Columbus, OH 43201
1	Brown University Division of Engineering ATTN: Prof. R. Clifton Providence, RI 02912
1	Georgia Institute of Technology ATTN: Dr. S. Atluri 225 North Avenue, NW Atlanta, GA 30332

DISTRIBUTION LIST

No. of Copies	Organization
1	Massachusetts Institute of Technology Aeroelastic and Structures Research Laboratory ATTN: Dr. E. A. Witmer Cambridge, MA 02139
1	Ohio State University Department of Engineering Mechanics ATTN: Prof. K. K. Stevens Columbus, OH 43210
3	Southwest Research Institute ATTN: Dr. H. N. Abramson Dr. W. E. Baker Dr. U. S. Lindholm 8500 Culebra Road San Antonio, TX 78228
1	Stanford Research Institute ATTN: Dr. W. Reuland 306 Wynn Drive, NW Huntsville, AL 35805
1	Texas A & M University Department of Aerospace Engineering ATTN: Dr. James A. Stricklin College Station, TX 77843
1	University of Alabama ATTN: Dr. T. L. Cost P.O. Box 2908 University, AL 35486
1	University of Delaware Department of Mechanical and Aerospace Engineering ATTN: Prof. J. R. Vinson Newark, DE 19711
	Aberdeen Proving Ground
	Marine Corps Ln Ofc Dir, USAMSAA ATTN: Dr. J. Sperrazza Mr. R. Norman, WSD Cmdr, USAEA ATTN: SAREA-MT-T Mr. R. Thresher Dr. D. Katsanis Mr. B. Jezek Mr. J. McKivrigan